C_{60} Aggregate Structure and Geometry in Nonpolar *o*-Xylene

Alok D. Bokare and Archita Patnaik*

Department of Chemistry, Indian Institute of Technology Madras, Chennai-600036, India

Received: July 6, 2004; In Final Form: October 26, 2004

Consequent to our recent papers on C_{60} colloidal aggregates in CS_2 solution (Bokare, A. D.; Patnaik, A. *J. Phys. Chem.* **2003**, *107*, 6079−6086) and their probable electron density distribution (Bokare, A. D.; Patnaik, A. *J. Chem. Phys.* **2003**, *119*, 4529−4538), the solution-phase structure of C_{60} in nonpolar *o*-xylene is reported using a positronium (Ps) atom as a fundamental probe, mapping changes in the local electron density of the microenvironment. Spontaneous formation of stable aggregates in the colloidal range (∼90−150 nm) was observed in a concentration range of 0.14−0.36 g/dm^3, beyond which they broke. An onset concentration for aggregate formation at 0.14 g/dm^3, as against 0.06 g/dm^3 for the polar CS_2 solvent, was noted and was substantiated by complete quenching of pyrene fluorescence at and beyond this onset due to photoinduced electron transfer from the pyrene excited state to the C_{60} aggregate. An order−disorder phase transition led to a notable geometry change of the colloidal particles; a sphere-to-nonuniform cylinder transition following an increase in the C_{60} concentration from 0.14 to 0.36 g/dm^3 revealed the aggregate curvature/internal modes to have been influenced by energetic/entropic and/or hydrodynamic interactions in the solvent medium. Transmission electron microscopy images of the aggregated clusters, in corroboration with Ps annihilation characteristics and pyrene fluorescence, revealed the clusters to be hexagonally close packed microcrystals.

Introduction

The all-carbon cage molecule fullerene (C_{60}) displays anomalous behavior in solution due to the formation of aggregates.[1−10] This behavior is attributed to a similar magnitude of specific surface energies of interaction among the C_{60} and solvent molecules. Aggregation of C_{60} has also been observed in heterogeneous media such as micelles,[11] liposomes,[12] and vesicles.[13] In homogeneous solvents, C_{60} aggregates have been extensively characterized in neat polar solvents and binary solvent mixtures and the aggregation process has been largely determined by the polarity of the medium.[6] In nonpolar aromatic solvents such as benzene[4] and toluene,[8] C_{60} aggregation was found to be a time-dependent slow process and the aggregates were unstable, even to mechanical shaking. Despite the existing literature in neat polar solvents, the aggregation phenomenon has not been confirmed in any other nonpolar aromatic solvent. Using a "positronium" (Ps) atom, a bound state of a free positron (e^+), and an electron (e^-) as a novel fundamental probe, this work is the first detailed report of the formation, growth, and structure of concentration-dependent stable C_{60} aggregates in neat *o*-xylene, establishing the critical (onset) concentration for aggregation to be 0.14 g/dm^3. The basis for employing this technique lies in the fact that the mechanism of Ps atom formation and its subsequent interaction with the medium are highly dependent on the physicochemical properties associated with locally different electronic environments. Locally different electronic structures, as a result of microscopic structure transformation or disorder and/or reorganization in the liquid structure, reflect an abrupt change in the annihilation spectral parameters, describing the *o*-Ps formation (I_3) and its lifetime (τ_3). The results from the present Ps annihilation spectroscopy (PAS) experiments are strongly corroborated with high-resolution transmission electron microscopy (HRTEM), fluorescence probe analysis, and UV−vis spectral measurements. Despite almost similar C_{60} solubilities in *o*-xylene and CS_2 solvents that have similar dielectric constants, a predominant solute−solvent interaction in *o*-xylene, on the basis of an aromatic and conjugated building block, has resulted in a drastic change in the aggregate structure and morphology.

Materials and Methods

C_{60} of 99.5+% purity was purchased from MER Corp., and the purity was confirmed through HPLC and mass spectrometry. *o*-Xylene, purchased from Sisco Research Laboratories, India, had stated a purity better than 98% and was distilled prior to use. C_{60} solutions in the concentration range 0.02−2.16 g/dm^3 were prepared by ultrasonication and degassed to remove the dissolved oxygen. Pyrene (99% pure) was received from Sigma Aldrich and used as received. Table 1 depicts solvent parameters for C_{60} molecules in CS_2 and *o*-xylene solvents.

Positron Lifetime Spectroscopy. Positron lifetime spectra were recorded by a fast−fast timing coincidence system consisting of BaF_2 scintillation detectors, with a timing resolution of 300 ps fwhm for a ^{60}Co prompt. A ∼15 μCi sodium-22 acetate positron source was sealed in thin Al foils of 2.5 μm thickness and was further wrapped in Kapton foils to avoid source leaking. The latter was dipped in the sample solution and spectral acquisition continued till 25K total counts under the peak were administered. The positron lifetime (τ) is a function of the electron density at the annihilation site. The annihilation rate (λ), which is the reciprocal of the positron lifetime τ, is given by the overlap of the positron density, $n_+(r) = |\Psi^+(r)|^2$, and the electron density, $n_-(r)$. The *o*-Ps−*p*-Ps conversion in a condensed medium occurs through electron exchange with the medium, and the lifetimes are dependent on the matrix structure and composition. Details of the acquisition and analysis of the lifetime spectra have been published

* To whom correspondence should be addressed. Fax: +91-44-22578241. E-mail: archita59@yahoo.com.

10.1021/jp047033b CCC: $30.25
Published on Web 12/07/2004

TABLE 1: Solubility of Fullerene (C_{60}) in *o*-Xylene and Carbon Disulfide at Room Temperature and the Associated Solvent Parameters (Vide References 7 and 14)

solvent	solubility (mg/mL)	dielectric constant (ϵ)	surface tension (σ) (dyn/cm)	viscosity (η) (cP)
o-xylene	8.70	2.57	29.76	0.81
carbon disulfide	7.90	2.64	31.58	0.36

previously.[1] Using necessary fitting programs, the *o*-Ps lifetimes and intensities were analyzed at various concentrations.

Transmission electron microscopy and selected area electron diffraction studies of the solutions were performed using a Philips STEM instrument (model SM12) equipped with a field emission gun operated at 120 kV. Microfilms for TEM studies were prepared by placing a drop of the solution on a carbon-coated copper grid and drying the solvent by evaporation at ambient temperature.

Fluorescence experiments with pyrene as a fluoroprobe were carried out with a Hitachi F-4500 spectrofluorimeter. The effective concentration of pyrene in all the C_{60} solutions was 1×10^{-5} M. The excitation wavelength was 310 nm, and the emission spectrum was scanned at wavelengths from 340 to 500 nm at an increment of 0.5 nm/s.

UV−Vis Absorption Spectroscopy. Electronic absorption spectra were recorded on a Cary 5E double-beam spectrophotometer using a 1 cm path length Infrasil cuvette. About 4 mL of the solution was placed in a 5 mL quartz cell, and the temperature of the solution was kept constant at 22 °C.

Results and Discussion

***o*-Ps Annihilation Characteristics in C_{60}−*o*-Xylene Solutions: Determination of the Critical Concentration for C_{60} Aggregation.** Figure 1a shows the *o*-Ps annihilation rate (λ_3) in the concentration range 0.02−2.16 g/dm^3, where the *o*-Ps lifetime ($1/\lambda_3$) increases with increasing C_{60} concentration and attains a maximum value. With a further increase in concentration, the lifetime decreases drastically till the maximum concentration, but with two different slopes. The minimum of the λ_3 curve (maximum τ_3) obtained at 0.14 g/dm^3 is attributed as the critical/onset concentration, C_{critical}, for stable C_{60} aggregate formation instantaneously upon C_{60} solubilization. On similar lines, a critical concentration of 0.06 g/dm^3 was obtained for the polar CS_2 solvent, as depicted in Figure 1b. At dilute concentrations of <0.14 g/dm^3 in Figure 1a, a decreasing trend in the rate/increasing *o*-Ps lifetime with respect to pure solvent implies a lower magnitude of local electron density around the *o*-Ps, and thus, a probable coexistence of C_{60} monomers and the pseudoaggregates is inferred. It has been pointed out[7] that, at concentrations 3 orders of magnitude lower than the saturation value, C_{60} clusters practically do not form and isolated molecules exist in the solution. The presence of a small fraction of C_{60} pseudoaggregates will contribute to the formation of nonequilibrated, loosely packed clusters and provide an opportunity for *o*-Ps localization in the open space within the pseudoaggregate, resulting in an increase in the *o*-Ps lifetime. Thus, even though the clusterization process has not reached equilibrium and the solution contains a large number of monomer species as compared to aggregates, the decrease in the annihilation rate (increasing lifetime) reveals that the *o*-Ps atom is already extremely sensitive to the formation of C_{60} aggregates. Beyond c_{critical}, a sharp enhancement in the rate is representative of the existence of C_{60} aggregates in the solution. The increased electron density due to the agglomeration of C_{60} molecules results in an efficient annihilation of the *o*-Ps and a lowering of its lifetime. This *o*-Ps annihilation behavior is also observed in aggregated systems such as microemulsions, where the *o*-Ps annihilation rate increased upon formation of normal and reverse micellar structures.[15,16]

The variation of the *o*-Ps annihilation rate over the entire C_{60} concentration range in the present work followed a linear relation according to $\lambda_3 = \lambda_p + k[C_{60}]$, with λ_p as the annihilation rate in the pure solvent and k the overall second-order rate constant, whose variation with C_{60} concentration is shown in Figure 1d. The rate constants are on the order of $\sim 10^{10}$ M^{-1} s^{-1}, and such high values, combined with the high electron affinity of C_{60}, show that the annihilation of *o*-Ps proceeds via the formation of a positronium−C_{60} electron donor−acceptor molecular complex:

$$2\gamma \xleftarrow{\lambda_p} Ps + C_{60} \underset{k_b}{\overset{k_f}{\rightleftarrows}} [Ps^+ - C_{60}^-] \xrightarrow{\lambda_C} C_{60} + 2\gamma$$

Pick-off annihilation from the solvent as a competing reaction gives rate constants on the order of $\sim 10^8$ M^{-1} s^1,[17] implying [Ps−C_{60}] complex formation to be the dominant annihilation mode.

Teller's[18] proposition that the curvature of C_{60} forces electrons to outside the cage, a larger electron density on the surface results, with the cage center becoming more positive. Consequently, a faster positron annihilation outside the cage was expected and was confirmed by bulk compressibility experiments.[19] Figure 1e shows the calculated electron density distribution in C_{60}, whose structure we optimized at the RHF/6-31G* level, using the Gaussian 98W program package.[20] The maximum electron density is observed to be localized on the surface of the molecule.

The *o*-Ps annihilation characteristics in C_{60}−benzene and C_{60}−toluene solutions revealed a concentration dependence of the annihilation rate, resulting from a strong electron scavenging action of C_{60}.[21] In carbon disulfide, although the *o*-Ps lifetime (τ_3) was shortened because of a larger electron density/dipole moment around the CS_2 molecule, owing to its high polarizability, the absolute *o*-Ps yield (in pure CS_2 solvent) was substantial (27.2%) and was found to be progressively quenched with increasing C_{60} concentration up to 14% at the maximum C_{60} concentration of 2.16 g/dm^3. However, the *o*-Ps quenching by C_{60} in *o*-xylene was not as pronounced as in CS_2; an absolute yield of 25.7% decreased to 16.8% at a concentration of 2.16 g/dm^3. This is attributed to the formation of C_{60}^- according to $C_{60} + e^- \rightarrow C_{60}^-$, which in turn inhibits the Ps formation process, withstanding the fact that electron abstraction from C_{60}^- is not feasible ($C_{60}^- + e^+ \neq C_{60} + Ps$). In CS_2, a stable structure of C_{60}^- is anticipated due to the charge polarization present as compared to the neutral xylenes, where only weak London forces prevail. The characteristic I_3 variation in Figure 1c further complies with that of λ_3 in Figure 1a.

Pyrene Fluorescence Characteristics in C_{60} Solutions: Confirmation of c_{critical}. Fluorescence probe analysis has been important in the biophysical studies of multimolecular aggregates such as micelles and membranes.[22] Pyrene is extensively used as the fluoroprobe due to its suitable photophysical properties, notably the long lifetime of its monomer and the fine structure (vibronic bands) in its monomer fluorescence spectrum in the solution phase. The intensities of these vibronic bands are strongly dependent on the solvent environment, and the use of the peak III/I emission intensity ratio to investigate micropolarity and to draw information on the existence of aggregated structures consisting of nonpolar hydrophobic domains has been well demonstrated.[23,24]

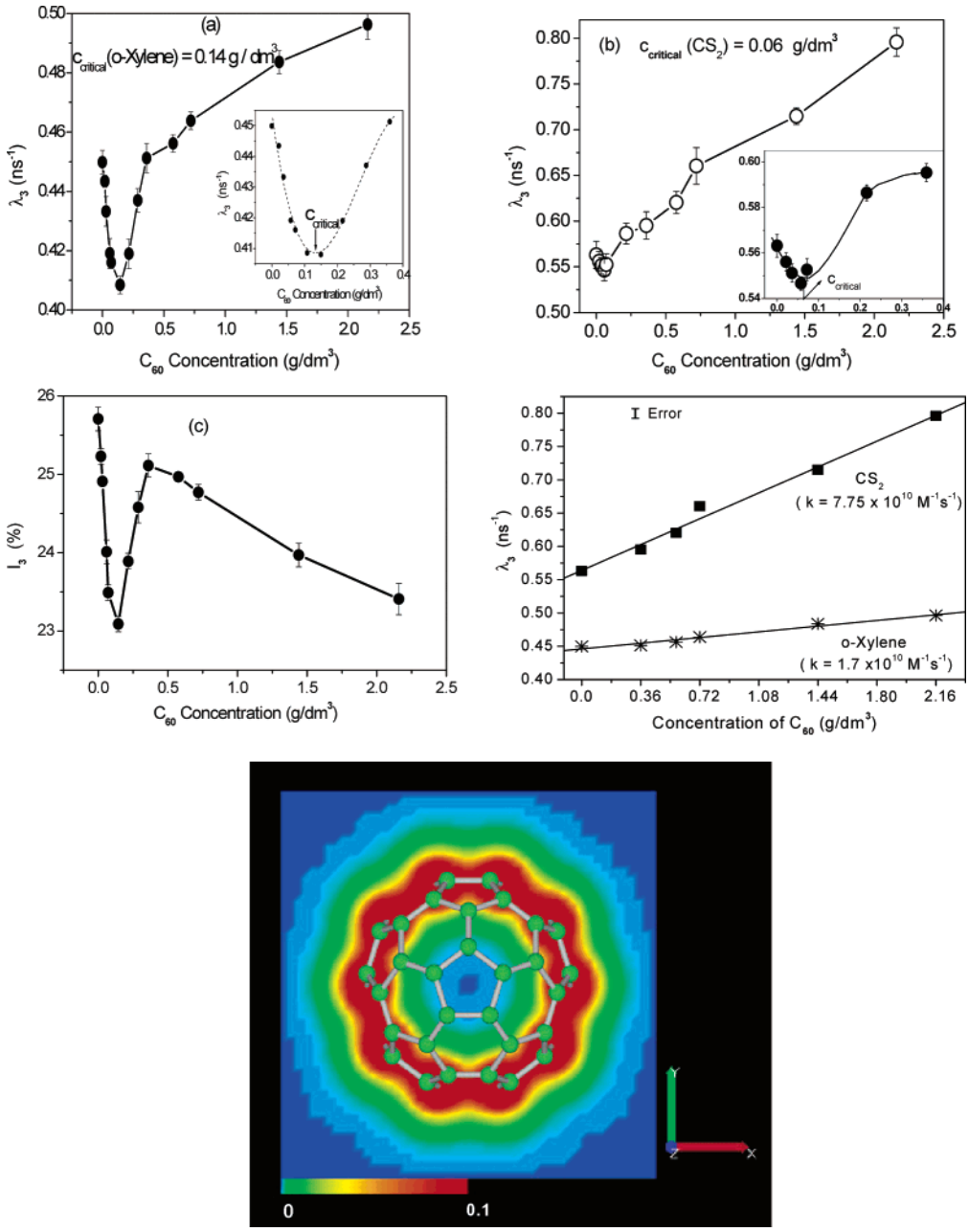

Figure 1. **(a)** Variation of the *o*-Ps annihilation rate (λ_3) with C_{60} concentration in *o*-xylene solvent. The inset shows the critical concentration ($c_{critical}$) for C_{60} aggregate formation, indicated by a minimum λ_3 at 0.14 g/dm^3. (b) Variation of λ_3 with C_{60} concentration in CS_2 solvent. **(c)** Variation of the *o*-Ps intensity (I_3) with C_{60} concentration in *o*-xylene solvent. **(d)** Variation of λ_3 with C_{60} concentration in different solvents (■, carbon disulfide; *, *o*-xylene. **(e)** Calculated electron density (e$^-$/au^3) distribution in geometry-optimized C_{60}, showing the maximum electron density on the surface.

Figure 2 shows the pyrene fluorescence spectrum of the C_{60} solutions in *o*-xylene at different concentrations. With an increase in the concentration of C_{60}, the emission intensity of the fluorophore decreases, and on approaching a concentration of 0.14 g/dm^3, the emission intensity is quenched rapidly, with no emission signal observed beyond this. The Stern−Volmer plot for fluorescence quenching of the 400 nm band is shown in the inset. The linear behavior of the Stern−Volmer plot at low C_{60} concentrations is attributed to the pyrene fluorescence quenching due to photoinduced electron transfer from pyrene to C_{60} with no significant energy-transfer process.

Previous studies on the use of pyrene as a probe to study C_{60} Langmuir−Blodgett films[25] showed that C_{60} is an efficient quencher of the pyrene monomer emission due to its high electron affinity. The efficiency of quenching at high C_{60} concentrations was found to be closer to unity. Thus, cluster formation in the present experimental solutions at and beyond the critical concentration (0.14 g/dm^3) would result in an efficient electron transfer from the pyrene excited state to the C_{60} hydrophobic cluster surrounding the localized pyrene molecule, leading to complete quenching. Any emission originating from C_{60} does not interfere, as the emission measurements were done in the wavelength range 350−600 nm, where C_{60} does not show any emission signals.[26] Thus, the use of pyrene emission characteristics indicated a threshold concentration of ∼0.14 g/dm^3 for C_{60} cluster formation in *o*-xylene, in excellent agreement with PAS.

Transmission Electron Microscopy of C_{60} Fullerene Aggregates. The structure of fullerene particles was studied by HRTEM. Figure 3 represents the high-magnification bright-field transmission electron micrographs of the 0.02 g/dm^3 C_{60} microfilm in *o*-xylene. Star-shaped structures with a dense center

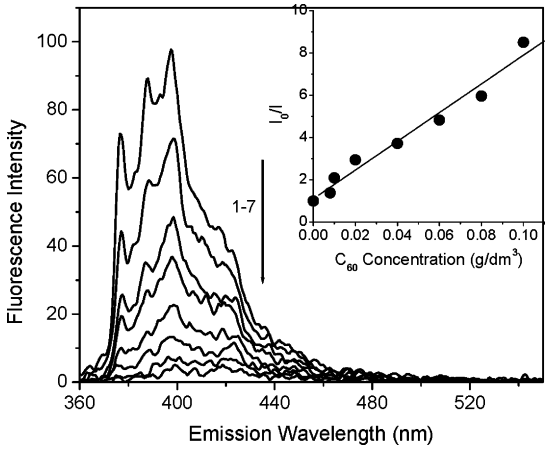

Figure 2. Emission spectrum of pyrene in C_{60} solutions in *o*-xylene as a function of C_{60} concentration. [C_{60}]: (1) 0.008 (2) 0.01 (3) 0.02 (4) 0.04 (5) 0.06 (6) 0.08 (7) 0.1 g/dm^3. The inset shows the Stern−Volmer plot of the fluorescence intensity ratio, I_0/I, of pyrene as a function of C_{60} concentration.

are observed in Figure 3a,b, with highly oriented electron diffraction pattern in Figure 3c. The discrete diffraction spots were analyzed to resemble a hexagonally close packed structure, indicating C_{60} to remain in the monomeric form at this concentration. At the critical/onset concentration of 0.14 g/dm^3, spherical assemblies were observed; Figure 4a shows a high-resolution image of the same with an average size of 95 nm, which increased with increasing concentration. The enlarged high-magnification image in Figure 4b shows the presence of individual C_{60} microdomains randomly oriented with respect to the neighboring domain.The electron diffraction of these aggregates taken from the same area as the image shows the presence of discrete spots, suggesting the C_{60} microdomains within the aggregate to have arranged themselves in a crystalline structure pattern, which is in contrast to the amorphous nature of the aggregates found in CS_2 medium at this concentration. With an increase in concentration, nonuniform cylindrical aggregates as multidomain structures up to a size of ∼140 nm with sufficient polydispersity were observed at 0.36 g/dm^3 (Figure 5). Further, as seen in Figure 5b, at the boundary of two angled grains, the aggregates maintain the periodicity of both grains; thus, a random arrangement of the crystal planes representing each microdomain within the aggregate is probable evidence for an isotropic association mechanism for clusterization of individual C_{60} crystallites, forming a nonspherical geometry of an approximate cylinder.

Understanding aggregate structure and morphology requires a description of its complex internal modes for which energetic, entropic, and hydrodynamic interactions must be accounted for. The curvature of aggregates in micellar systems has been seen to be influenced by the headgroup interactions with water and with each other. Surface aggregates of zwitterionic surfactant dodecyldimethylammoniopropanesulfonate have shown greater curvature on mica and silicon nitride than on graphite, supporting the hypothesis that surface aggregates are less curved on hydrophobic surfaces.[27] For a given concentration, a lower aggregate curvature reduces the area of interaction between the hydrophobic solid and water, resulting in the coverage of a larger surfactant area. The latter suggests a larger size of the surface aggregate on hydrophobic surfaces as compared to hydrophilic ones. Pronounced structure variations were also noted; the tetradecyltrimethylammonium bromide aggregates on hydrophobic mica were found to be long and hemicylindrical, whereas on hydrophilic silica, spherical geometry was observed. In line

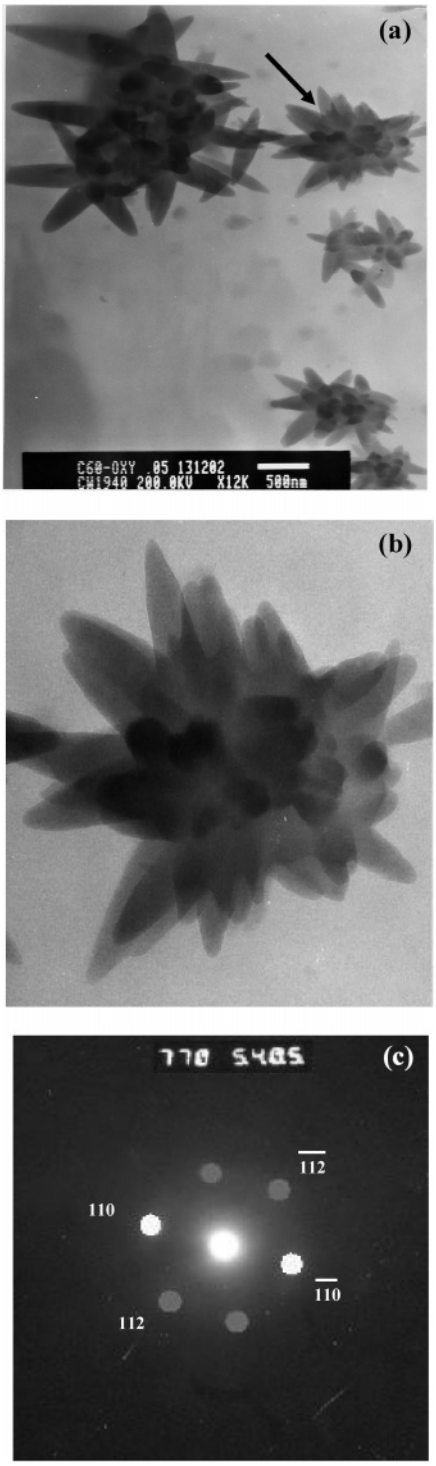

Figure 3. TEM images of the 0.02 g/dm^3 C_{60} microfilm in *o*-xylene showing the **(a)** low-magnification and **(b)** the enlarged portions of the marked star-shaped single crystals. **(c)** illustrates the electron diffraction pattern of the star-shaped structures as shown in (a) and (b).

with the above, in the present study, bulk C_{60} aggregates in the hydrophobic *o*-xylene showed a slightly larger size and lower curvature in comparison to those observed in polar CS_2.[1] There are at least two structural changes consistent with the observation: (i) a lower aggregate curvature and (ii) an increase in aggregate separation (Figure 5). Aggregation phenomena here are a function of two opposing effects: association to reduce hydrophobic interactions [$(C_{60})_n$−*o*-xylene, $(C_{60})_n$−$(C_{60})_n$] and Coulombic repulsion between $(C_{60})_n$ and $(C_{60})_n$. The latter is due to the fact that the charge density distribution in $(C_{60})_n^2$

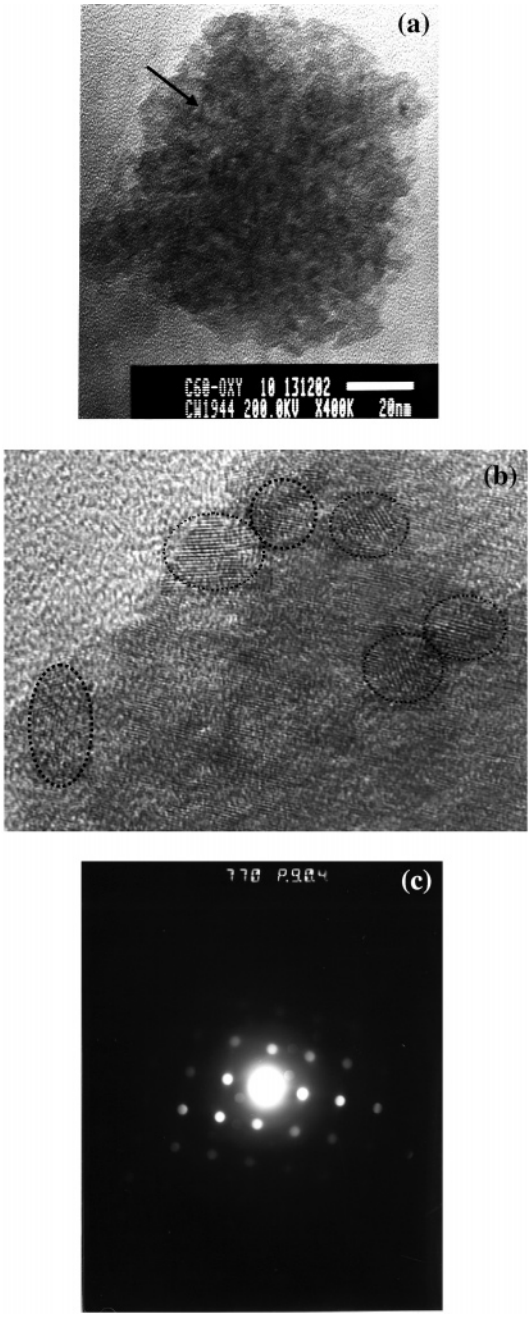

Figure 4. **(a)** HRTEM image of the 0.14 g/dm^3 C_{60} solution microfilm. (b) shows the enlarged image of a section of the aggregate (highlighted) in (a) and depicts the crystal planes representing individual C_{60} microdomains. **(c)** represents the micro diffraction pattern of the aggregated clusters at the critical concentration 0.14 g/dm^3.

resembles that in a C_{60} monomer, where the total density lies at the periphery of the cage. In the presence of a relatively less polar/lower dielectric constant solvent, *o*-xylene, the Coulombic repulsions are not screened, thus leading to a larger area, a lower curvature, and distantly separated aggregates, as seen in Figure 5. A difference in the dielectric constant of the solvent used would change the above-mentioned interactions accordingly with a change in entropy and the morphology of the aggregate structure.

Solvent Effect on the Aggregate Structure and Morphology, Studied through UV−Vis Spectroscopy. From the above discussions it is evident that C_{60} aggregation in aromatic *o*-xylene shows an *o*-Ps annihilation rate (λ_3) behavior[1,2] similar to that found in CS_2 solvent as a function of C_{60} concentration

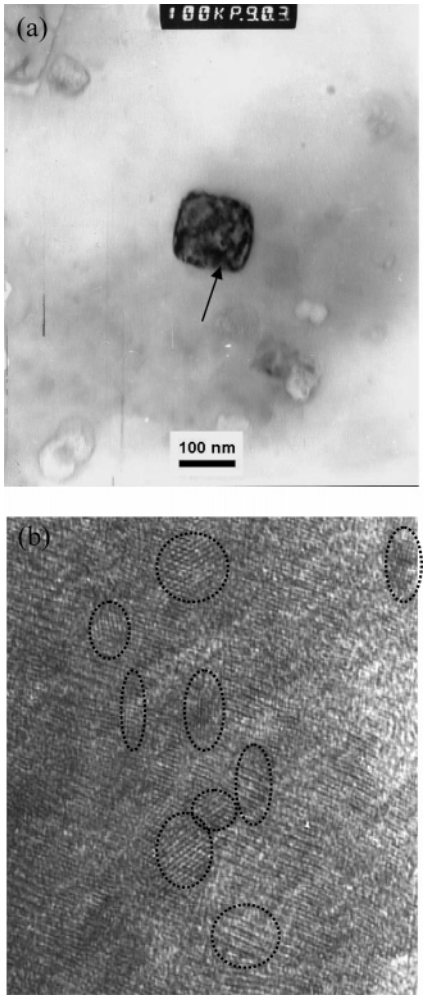

Figure 5. (a) HRTEM image of the 0.36 g/dm^3 C_{60} solution microfilm. (b) shows the enlarged portion of a section of the aggregate.

in a similar concentration range. However, the TEM results for C_{60} aggregates in CS_2 showed amorphous, spherical aggregates, which followed a fractal growth at the critical concentration.[1] Moreover, a lower onset concentration for aggregation (0.06 g/dm^3) was obtained in CS_2. These sharp contrasts in the properties of the C_{60} aggregates in two different kinds of solvents reveal the crucial role of the solvent in deciding the nature and morphology of the aggregates.

The nature of the solute−solvent interactions governs the growth and structure of the C_{60} aggregates. UV−Vis absorption studies of the interaction between C_{60} and the aromatic solvent molecules in CCl_4 as a medium are shown in Figure 6. With increasing concentration of the solvents, there is a progressive increase in the C_{60} absorbance band in the 450−650 nm region, accompanied by solvatochromism in the 328 nm band, indicating the presence of ground-state interaction between the fullerene and the solvent molecules. Similar features were also observed for C_{60}−CS_2 in CCl_4. However, the modes of interaction are different in the two cases. The C_{60}−CS_2 interaction proceeds through the diffuse electron density or polarizability on CS_2, stabilizing the electronic transitions. In the case of aromatic *o*-xylene, π-stacking of the electron cloud on C_{60} and xylene is the dominant mode of interaction.[28] This mode of interaction is more efficient than that between C_{60} and CS_2, as observed by the higher solubility of C_{60} in *o*-xylene than in CS_2.[7] The higher electron-donating nature of methyl-substituted solvents compared to unsubstituted aromatic solvents such as benzene also provides evidence for an efficient π-stacking interaction

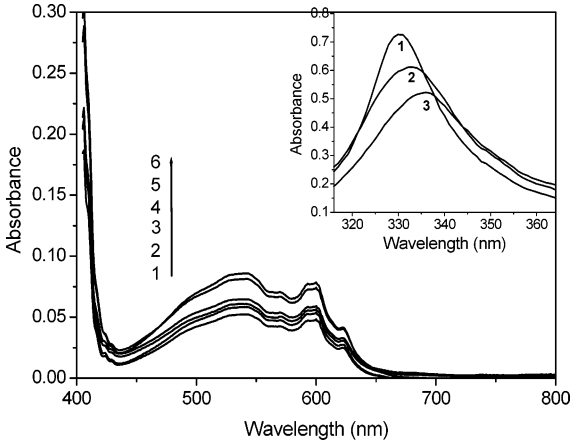

Figure 6. Absorption spectrum of C_{60} (1.0×10^{-4} M in CCl_4, 1 cm cell) in the presence of *o*-xylene. [*o*-Xylene]: (1) 0.000 (2) 0.164 (3) 0.328 (4) 0.492 (5) 0.656 (6) 0.820 M. The inset shows the 328 nm band of C_{60} in CCl_4−*o*-xylene mixtures. The mole fractions of *o*-xylene are (1) 0.00, (2) 0.5, and (3) 1.0.

in *o*-xylene compared to toluene, which is reflected in a higher C_{60} solubility in *o*-xylene with respect to toluene. The strong solute−solvent interactions in *o*-xylene also explain the higher critical concentration for C_{60} aggregation compared to that in CS_2, as evidenced from the PAS results. An increasing number of C_{60} monomers is required to overcome the strong solute−solvent interactions as a result of structure similarity in C_{60} and *o*-xylene, thus strengthening the weak van der Waals force between two C_{60} molecules toward the formation of stable aggregates.

Conclusion

Combination of self-assembly on a length scale of a few nanometers has led to structural hierarchies, based on phase transitions of the assembled structures. In the present work, concentration-dependent structure attribution to C_{60} aggregates in *o*-xylene solvent medium was accomplished from a microscopic picture of the Ps surroundings in the solution and from TEM and further supported by pyrene fluorescence quenching studies. At dilute concentrations, before the critical point, the system remained as an isotropic liquid with C_{60} monomers and monomers tended to aggregate but could not because of instability or nonattainment of an equilibrium state. Localization of *o*-Ps within these pseudoaggregates resulted in an increase in its lifetime and underlined its sensitivity to probe the aggregation phenomenon. With increasing concentration, just at or after the onset of aggregation, the spherical clusters were stabilized owing to strong intermolecular interactions. Association of the microdomains within the aggregates resulted in a crystalline packing. The crucial role of the solvent in governing the aggregation process was discussed; a change from a higher polarity (CS_2) to a lower polarity (*o*-xylene) solvent resulted in a structure transition from a sphere to a nonuniform cylinder with sufficient polydispersity. With a pronounced size variation at a concentration of 0.36 g/dm^3, the threshold concentration for aggregate formation and the aggregate growth mode, the shape, and crystallinity differed enormously in *o*-xylene.

Acknowledgment. This work was supported by the Department of Science and Technology (DST), Government of India, Grant No. SP/S1/H-37/2001.

References and Notes

(1) Bokare, A. D.; Patnaik, A. *J. Phys. Chem.* **2003**, *107*, 6079−6086.
(2) Bokare, A. D.; Patnaik, A. *J. Chem. Phys.* **2003**, *119*, 4529−4538.
(3) Sun, Y.-P.; Bunker, C. E. *Nature* **1993**, *365*, 398.
(4) Ying, Q.; Marecek, J.; Chu, B. J. *J. Chem. Phys.* **1994**, *101*, 2665−2672.
(5) Ghosh, H. N.; Sapre, A. V.; Mittal, J. P. *J. Phys. Chem.* **1996**, *100*, 9439−9443.
(6) Nath, S.; Pal, H.; Palit, D. K.; Sapre, A. V.; Mittal, J. P. *J. Phys. Chem. B* **1998**, *102*, 10158−10164.
(7) Bezmel'nitsyn, V. N.; Eletskii, A. V.; Stepanov, E. V. J. *Phys.-Usp.* **1998**, *41*, 1091−1114; *J. Phys. Chem.* **1994**, *98*, 6665−6667.
(8) Bulavin, L. A.; Adamenko, I. I.; Yashchuk, V. M.; Ogul'chansky, T.Yu; Prylutskyy, Yu. I.; Durov, S. S.; Scarff, P. *J. Mol. Liq.* **2001,** *93*, 187−191.
(9) Yevlampieva, N. P.; Birulin, Y. F.; Melenevskaja, E. V.; Zgonnik, V. N.; Rjumtsev, E. I. *Colloids Surf., A* **2002**, *209*, 167−171.
(10) Alargova, R. G.; Deguchi, S.; Tsujii, K. *J. Am. Chem. Soc.* **2001**, *123*, 10460−10467.
(11) Hungerbühle, H. R.; Guldi, D. M.; Asmus, K. D. *J. Am. Chem. Soc.* **1993**, *115*, 3386.
(12) Bensasson, R. V.; Bienvenue, E.; Dellinger, M.; Seta, S. J. *J. Phys. Chem.* **1994**, *98*, 3492−3500.
(13) Janot, J. M.; Bienvenue, E.; Seta P.; Bensasson, R. V.; Tome, A. C.; Enes, R. F.; Cavaleiro, J. A. S.; Camps, S. X.; Hirsch, A. *J. Chem. Soc., Perkin Trans.* **2000**, *22*, 301−306.
(14) Lide, D. R. *Handbook of Chemistry and Physics*, 83rd ed.; CRC Press: Boca Raton, FL, 2002.
(15) Boussaha, A.; Djermouni, B.; Fucugauchi, L. A.; Ache, H. J. *J. Am. Chem. Soc.* **1980**, *102*, 4654−4658.
(16) Duplâtre, G.; Ferreira Marques, M. F.; da Graça Miguel M. *J. Phys. Chem.* **1996**, *100*, 16608−16612.
(17) Ache, H. J. *Positronium and Muonium Chemistry*; American Chemical Society: Washington, DC, 1979.
(18) Teller, E. *Mater. Sci. Forum* **1992**, *105−110*, 161−168.
(19) Duclos, S. J.; Brister, K.; Haddon, R. C.; Krotan, A. R.; Thiel, F. A. *Nature* **1991**, *351*, 380−382.
(20) Frisch, M. J.; et al. *Gaussian 98*, revision A.9; Gaussian Inc.: Pittsburgh, 1998.
(21) Sundar, C. S.; Premila, M.; Gopalan, P.; Hariharan, Y.; Bharathi, A. *Fullerene Sci. Technol.* **1995**, *3* (6), 661−679.
(22) Gratzel, M.; Thomas, J. K. *Modern Fluorescence Spectroscopy*; Plenum Press: New York, 1976; Vol. 2.
(23) Zana R.; In *Surfactant Solutions: New Methods in Investigation*; Zana, R., Ed.; Marcel Dekker: New York, 1987.
(24) Thomas, J. K. *Chem. Rev.* **1980**, *80*, 283.
(25) Sluch, M. I.; Samuel, I. D. W.; Petty, M. C. *Chem. Phys. Lett.* **1997**, *280*, 315.
(26) Ma, B.; Sun, Y.-P. *J. Chem. Soc., Perkin Trans.* **1996**, *2*, 2157.
(27) William, A. D.; Grant, L. M. *J. Phys. Chem.* **1996**, *100* (28), 11808−11811.
(28) Ceolin, R.; Michaud, F.; Toscani, S.; Agafonov, V.; Tamarit, J. L.; Dworkin, A.; Szwarc, H. *Recent Advances in Chemistry and Physics of Fullerenes and Related Materials*; Pennington, NJ, 1997.